

STING is significantly increased in high-grade glioma with high risk of recurrence

Meishi Zhong*, Manmei Long*, Chenjie Han, Saiyan Ji, and Qingyuan Yang 

Department of Pathology, Shanghai Ninth People's Hospital, Shanghai Jiao Tong University School of Medicine, Shanghai, China

ABSTRACT

In this study, we aimed to comprehensively characterize the potential relationships among the frequently mutated genes, well-known homologous recombination repair (HRR) proteins, and immune proteins in glioma from a clinical perspective. A total of 126 surgical tissues from patients initially diagnosed with glioma were included. The genetic alterations were tested using the targeted next-generation sequencing technique. The expression of HRR proteins, immune proteins, and genetic alteration-related proteins were detected using immunostaining. Integrated analysis showed that ATRX is positively correlated with STING in high-grade glioma (HGG) with wild-type ATRX and IDH1. Then, a relapse predictive risk-scoring model was established using the least absolute shrinkage and selection operator regression algorithms. The scores based on the expression of ATRX and STING significantly predict the recurrence for glioma patients, which further predict the survival for specific subgroups, characterized with high expression of RAD51 and wild-type TERT. Moreover, STING is significantly higher in patients with high relapse risk. Interestingly, STING inhibitors and agonists both suppress the growth of HGG cells, regardless of their STING levels and STING pathway activity, whereas RAD51 inhibitor B02 is found to exclusively sensitize HGG cells with high expression of STING to temozolomide *in vitro* and *in vivo*. Overall, findings in the study not only reveal that ATRX is closely correlated with STING to drive the relapse of HGG, but also provide a STING-guided combined strategy to treat patients with aggressive gliomas. Translation of these findings will ultimately improve the outcomes for ATRX and IDH1 genomically stratified subgroups in HGG.

ARTICLE HISTORY

Received 1 August 2023
Revised 1 March 2024
Accepted 4 March 2024

KEYWORDS

ATRX; high-grade glioma; IDH1; RAD51 inhibitor; STING; temozolomide sensitivity

Introduction

Around 80% of malignant brain tumors are diagnosed as glioma.¹ Previously, the World Health Organization (WHO) has classified gliomas by grades based on their pathological features, with grades I and II representing low-grade glioma (LGG), and grades III and IV representing high-grade glioma (HGG).² Presently, they suggest that molecular phenotypes should be integrated into their classification to guide more precise treatments.² However, recurrence, which appears within 6–9 months after initial diagnosis, is still the most lethal factor causing poor survival in glioma.³

The genetic landscape in glioma has been mapped for decades, with telomerase reverse transcriptase (TERT), tumor protein p53 (TP53), isocitrate dehydrogenase 1/2 (IDH1/2), alpha-thalassemia, mental retardation, X-linked (ATRX) frequently mutated in adult glioma⁴ and H3-3A commonly mutated in pediatric glioma.⁵ Multiple studies have been performed to interpret the clinical significance of these mutations. For instance, ATRX mutations are strongly correlated with IDH mutations and TP53 mutations, which are mutually exclusive to mutations in the promoter of TERT (TERT^{PRT}).⁶ In addition, genetic alterations have been reported to play crucial roles in modulating DNA damage repair (DDR), immune response, cell growth, and chemosensitivity in glioma,⁴ however, there are still no integrated studies focusing

on characterizing their complex relationships from clinical perspectives.

Emerging evidence support that alterations of DDR factors result in distinct immune phenotypes and cytokine profiles in glioma. For instance, upon intrinsic and extrinsic DNA damage, the cytosolic DNA induces the activation of cyclic GMP-AMP synthase (cGAS)-stimulator of interferon genes (STING), also known as TMEM173, signaling to trigger the production of type I interferons (IFNs) and pro-inflammatory cytokines through IFN regulatory factor-3 (IRF3) and NF-κB activation in tumor immune microenvironment (TIME), which is a well-known pathway mediating the crosstalk between DDR, specifically the homologous recombination repair (HRR), and immune responses in solid tumors.⁷ However, the complex features among them in glioma have not been clinically studied.

Herein, in this study, we performed an integrated study of clinicopathology, frequent mutations of ATRX, IDH1, H3-3A, and TERT^{PRT}, mutation-related proteins ATRX and IDH1 (R132H), HRR proteins RAD51 and γH2AX, and immune proteins cGAS, STING, and PD-L1 in glioma to comprehensively characterize their relationships, and further explored their potential treatments. Interestingly, our data showed that ATRX is positively correlated with STING in HGG with wild-type ATRX and IDH1 (ATRX^{wt}/IDH1^{wt}), rather than that in LGG with mutant ATRX and IDH1 (ATRX^{mut}/IDH1^{mut}). Then,

CONTACT Qingyuan Yang  shengzhou-2005@163.com  Department of Pathology, Shanghai Ninth People's Hospital, Shanghai Jiao Tong University School of Medicine, No. 639, Manufacturing Bureau Road, Shanghai 200011, China

*These authors equally contributed to the study.

 Supplemental data for this article can be accessed online at <https://doi.org/10.1080/2162402X.2024.2327682>

© 2024 The Author(s). Published with license by Taylor & Francis Group, LLC.

This is an Open Access article distributed under the terms of the Creative Commons Attribution-NonCommercial License (<http://creativecommons.org/licenses/by-nc/4.0/>), which permits unrestricted non-commercial use, distribution, and reproduction in any medium, provided the original work is properly cited. The terms on which this article has been published allow the posting of the Accepted Manuscript in a repository by the author(s) or with their consent.

a relapse predictive risk-scoring model was successfully established using the least absolute shrinkage and selection operator regression (LASSO) algorithm based on the expression of ATRX and STING. The scores significantly predict the recurrence for glioma patients, which are externally validated using datasets from the Chinese Glioma Genome Atlas (CGGA). Moreover, the scores specifically predict survivals for patients with high expression of RAD51 and wild-type TERT (TERT^{wt}). And STING is also highly increased in patients with high relapse risk. Results from therapeutic explorations demonstrated that both STING inhibitors and agonists significantly suppress the growth of HGG cells, regardless of their STING levels and STING pathway activity, whereas RAD51 inhibitor B02 exclusively sensitizes HGG cells with high expression of STING to temozolomide (TMZ) treatments *in vitro* and *in vivo*. Overall, findings in the study not only reveal that ATRX is closely correlated with STING to drive the relapse of HGG, but also provide a STING-guided combined strategy to treat patients with aggressive gliomas. Translation of these findings will ultimately improve the outcomes for ATRX and IDH1 genomically stratified subgroups in HGG.

Materials and methods

Study population, follow-up, and ethics

The archived formalin-fixed paraffin-embedded (FFPE) blocks of surgical samples from patients primarily diagnosed with glioma during their first visit to Wuhan Central Theater Command General Hospital (CTCGH) between January 2015 and December 2019 were included in the study. Accordingly, a total of 126 FFPE blocks with one block per patient were finally included. The postoperative follow-up of survival and relapse status was performed by clinicians in March 2022, with a median follow-up period of 59 months. And 55 patients were out of contact. The clinicopathological information was retrieved from the hospital electronic information system. This study was approved by the Institutional Research Ethics Committee of CTCGH (Protocol no. [2022]009-01).

Cell culture and treatments

The HGG cell lines U87, U251, LN229, H4, A172, TJ905, and SW1783 were all commercially purchased from the BeNa Culture Collection (BNCC[®], CN), which were most recently authenticated using the short-tandem repeat profiling approach in 2021 and periodically tested mycoplasma negative. Cells were all cultured in Dulbecco Modified Eagle Medium supplemented with 10% fetal bovine serum and 1% penicillin/streptomycin in a humidified incubator with 5% CO₂ at 37°C. In the study, H4 cells were pre-treated with vehicle (0.1% DMSO) or 10 μM diABZI for 6 h or 10 μM SN-011 for 12 h, U87 and A172 cells were pre-treated with vehicle or 1 μM diABZI or 10 μM SN-011 for 6 h.

Targeted next-generation sequencing

The genomic alterations of ATRX, IDH1, H3-3A at exon regions and of TERT^{PRT} were commercially tested by

Homgen[®] (Shanghai, CN) with targeted next-generation sequencing (NGS) technique. In brief, the genomic DNA ($n = 126$) was extracted from above FFPE blocks using the AllPrep DNA/RNA FFPE kit (#80234, QIAGEN, Germany), which was then sonicated into 200–350 bp in length. According to the manufacturer's most recent protocol (V3-20220313, Homgen[®], Shanghai, CN), the sequencing library was prepared, concentrated, hybridized with JY4 probe panel, captured with ProbeCap[®] SA beads, washed and purified in turn. Finally, the library was quantified using the 2100 bioanalyzer (Agilent, USA) and sequenced on the Novaseq 6000 Fellcell-S4PE150 platform (Illumina, USA). The FASTQ files were then aligned to the hg19 genome, and the mutations were called according to the manufacturer's standard bioinformatics pipeline (Homgen[®], CN). Noteworthy, the original FASTQ files of all the specimens were deposited in the National Genomics Data Center (NGDC) under the accession number PRJCA012429.

Tissue microarray construction and immunostaining

One core per FFPE block with sufficient glioma cells was constructed on a tissue microarray (TMA). Afterward, the TMA block was continuously sliced into 3–5-μm-thick slides for downstream immunohistochemistry (IHC) staining, which were automatically performed on the Benchmark Ultra instrument (Roche, USA). Finally, the proteins were stained brown with HRP-mediated reaction of 3,3-diaminobenzidine. The detailed information of primary antibodies used for IHC assays was summarized in Table S2.

In terms of expression interpretation, the immunoreactive score (IRS), a multiplication product of the percentage of positive tumor cells and intensity of staining,⁸ was calculated based on assessments from two independent pathologists. Additionally, the expression of ATRX, RAD51, cGAS, STING, γH2AX, and H3K27me3 was further considered as low or high when IRS < 5 or IRS > 5, while the IDH1 (R132H) was defined as negative when IRS = 0, otherwise it was positive according to the receiver operator characteristic (ROC) curve analysis of its prediction for IDH1^{R132H} mutation. As for PD-L1, its expressions were considered negative or positive when the combined positive score (CPS) < 1% or ≥ 1%.⁹

Public datasets

The genetic mutations of ATRX and IDH1 in glioma tissues with survival data were downloaded from cBioPortal database.¹⁰ The RNA-seq data of ATRX and STING shown as RSEM from two independent cohorts with recurrence status were downloaded from CGGA (CGGA_325 and CGGA_693).^{11,12}

Correlation matrix analysis and establishment of relapse predictive risk-scoring model

The correlation matrix analysis of all the protein levels shown as IRS was performed using the Corrplot package (version 0.92) in R studio with specific arguments (sig.level = 0.05, insig

= 'blank', order = 'hclust', addrect = 4). The LASSO regression algorithm was used to establish the best scoring model predicting the relapse risk using the glmnet package (version 4.1–4) in R Studio. The risk score was calculated following the formula: risk score = $\sum_1^n \text{Coef}(i) * \exp(i)$, with Coef (i) meaning the coefficient of each variable and exp (i) representing the expression level of the corresponding variable.

In vivo therapeutic tumor-bearing animal study

Thirty male NOD SCID mice aged 6 to 7 weeks were ordered from Ziyuan Co., Ltd (Hangzhou, CN) and maintained at Chedun Co., Ltd (Shanghai, CN) for the *in vivo* therapeutic experiments according to the Laboratory Animal License approved by Shanghai Science and Technology Commission [SCXK(Shanghai)2022–0001]. The mice were randomly divided into two groups, namely LN229 group ($n = 15$) and H4 group ($n = 15$), respectively. Afterward, 5×10^6 LN229 or H4 cells per mice mixed with matrigel were subcutaneously injected into the right flanks of mice in the indicated groups. When the tumor volumes ($0.5 \times \text{length} \times \text{width}^2$) reached to around 100 mm^3 , the mice with LN229 or H4 cells were further divided into three subgroups intraperitoneally administered with indicated drugs twice per week, vehicle ($n = 5$), 50 mg/kg TMZ ($n = 5$),¹³ 50 mg/kg TMZ plus 25 mg/kg B02 ($n = 5$).¹⁴ The body weights (g) and tumor volumes (mm^3) were recorded accordingly. Finally, the study was terminated when tumor volumes in the vehicle group reached the ethical approved maximum volume of 2000 mm^3 , and the xenografts were kindly removed, weighted, and pictured according to the approved protocol (SH9H–2022–A326–SB) by the Laboratory Animal Ethics Committee of Shanghai Ninth People's Hospital, Shanghai Jiao Tong University School of Medicine.

Statistics

In this study, the ROC curve was used to assess the predictive reliability. The univariate and multivariate Cox regression analysis was performed to identify independent prognostic markers. The Students' *t*-test and the one-way ANOVA test were applied to study the difference in groups ($n = 2$) and groups ($n \geq 3$), respectively. The Kaplan–Meier (KM) curve was used to analyze the OS difference between the two groups. The Chi-square (χ^2) test was used to evaluate the categorical data. Statistical analysis was performed using either GraphPad Prism version 8.0 or SPSS statistics (version 25.0). The significance was considered when the two-sided $p < 0.05$, which was further classified into four levels, $p < 0.05$, $p < 0.01$, $p < 0.001$, and $p < 0.0001$.

Results

Multi-facet characteristics of the study population

In the study, a total of 126 surgical FFPE blocks from glioma patients with one block per patient were included. However, 55 patients were out of contact. Accordingly, the population was then defined as the overall cohort with 126 patients and the discovery cohort with 71 patients who had the follow-up

information (Figure 1). The representative low and high expressions of the studied proteins are shown in Figure S1A.

Immunostaining of ATRX and IDH1 (R132H) has been suggested as surrogate markers for ATRX and IDH1^{R132H} mutations, respectively.¹⁵ In line with these reports, our data also support that ATRX^{IRS} significantly predicted for ATRX frameshift mutations (ATRX^{fs}), which contribute to its protein loss,¹⁶ with an area under the curve (AUC) of 0.7433 (Figure S1B, $p = 0.0008$). While IDH1 (R132H)^{IRS} predicted for its IDH1^{R132H} with an AUC of 0.7933 (Figure S1C, $p < 0.0001$), consolidating the accuracy of our evaluation system.

In the overall cohort, 42.1% patients were diagnosed with LGG, while 57.9% were with HGG (Table S3). Noteworthy, 8.7% pediatric gliomas were also included in the study. Interestingly, the HRR proteins were highly expressed in gliomas, shown to be 86.2% tissues with high expression of γ H2AX, 76.8% with high expression of RAD51, and 60.8% with high expression of ATRX (Table S3), implicating that the HRR factors are promising targets. Contrary to the HRR proteins, the immune proteins were lowly expressed, shown to be 87.4% tissues with low expression of cGAS, 75.0% with low expression of STING, and up to 93.9% with negative PD-L1 (Table S3), suggesting that cGAS and PD-L1 targeted immunotherapies possibly benefit limited glioma patients, except for STING. Of note, the frequency of genetic mutations of ATRX, IDH1, H3-3A, and TERT^{PRT} were same as previous reports,⁴ shown as 31.0% tissues with TERT^{PRT} mutations, 34.9% with ATRX^{mut}, 28.6% with IDH1^{mut}, and 6.3% with H3-3A^{mut} (Table S3). Additionally, the above multi-faceted features in the discovery cohort were not statistically different from those in the overall cohort (Table S3). Taken together, the characteristics of our studied population are consistent with those of glioma patients worldwide.

ATRX and STING are highly expressed in HGG characterized with wild-type ATRX and IDH1

Next, our integrated analysis showed that ATRX and STING were significantly downregulated in glioma tissues with mutant ATRX (ATRX^{mut}), compared to those with wild-type ATRX (ATRX^{wt}) (Figure 2a, $p = 0.001$ for ATRX, and $p = 0.0056$ for STING). More specifically, the downregulation of ATRX was attributed to ATRX^{fs} mutations (Figure 2b, $p = 0.0018$), whereas the decrease in STING was induced by missense mutations of ATRX (ATRX^{mis}) (Figure 2b, $p = 0.0325$). Similarly, the expressions of ATRX and STING were both significantly lower in tissues with IDH1^{mut} than those with IDH1^{wt} (Figure 2c, $p = 0.0005$ for ATRX, and $p = 0.0104$ for STING). In line with data in Figure S1C, IDH1 (R132H) was highly expressed in tissues with IDH1^{mut} (Figure 2c, $p = 0.0012$). However, ATRX and STING were not differentially expressed in tissues with TERT^{wt} and TERT^{PRT} mutations (Figure 2d). Previous studies have reported that the mutations of ATRX and IDH1 are mutually exclusive to TERT mutations in glioma,⁶ therefore, we propose that the downregulation of ATRX and STING is also exclusive to ATRX and IDH1 mutations.

Subsequently, the overall cohort was stratified into four subgroups based on the genetic alterations of ATRX and

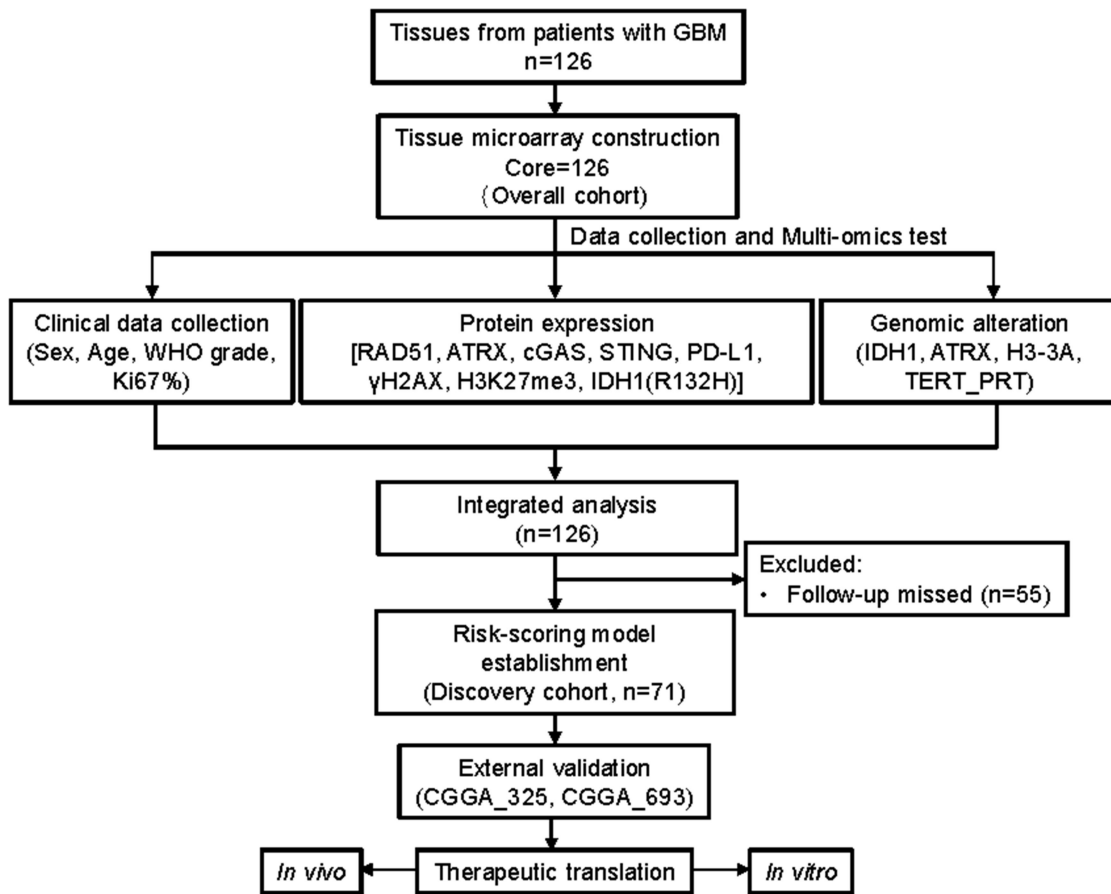


Figure 1. Work flowchart of this clinical and translational study.

IDH1, namely ATRX^{wt}/IDH1^{wt}, ATRX^{wt}/IDH1^{mut}, ATRX^{mut}/IDH1^{wt}, ATRX^{mut}/IDH1^{mut}. Interestingly, ATRX and STING were both significantly downregulated in tissues with ATRX^{mut}/IDH1^{mut}, compared to those with ATRX^{wt}/IDH1^{wt} (Figure 2e, $p = 0.0003$ for ATRX, and $p = 0.0161$ for STING). Further analysis revealed that ATRX and IDH1 genetically stratified subgroups were closely correlated with WHO grade ($p = 0.015$), ATRX ($p = 0.001$), STING ($p = 0.041$), and IDH1 (R132H) ($p < 0.0001$) (Figure 2f and Table 1). In particular, ATRX^{mut}/IDH1^{mut} was enriched in LGG, while ATRX^{wt}/IDH1^{wt} was common in HGG (Figure 2g and Table 1). And the prognostic results from cBioportal¹⁰ showed that patients with ATRX^{wt}/IDH1^{wt} had poorer survival rates than those with ATRX^{mut}/IDH1^{mut} (Figure 2h, hazard ratio [HR] = 4.134, 95% confidence interval [CI]: 3.679 to 4.645, $p < 0.0001$). Taken together, we speculate that the high expression of ATRX and STING in HGG characterized with ATRX^{wt}/IDH1^{wt}, which is categorized as glioblastoma (GBM) by WHO,¹⁷ possibly contributes to glioma malignant progression.

ATR^X and STING are positively correlated to drive the relapse in GBM

Afterward, the mutual correlation analysis among HRR proteins, immune proteins, and genetic alteration-related proteins revealed two closely correlated clusters, one was composed of ATRX and STING, the other one was composed of γ H2AX,

RAD51, and H3K27me3 (Figure 3a). Moreover, STING was significantly upregulated in glioma tissues with ATRX^{high}, compared to those with ATRX^{low} (Figure 3b, $p = 0.0007$). Previous studies have shown that deficiency of ATRX results in a reduced adaptive immune response, marked by the downregulation of cGAS-STING signaling in response to radiation in sarcoma.¹⁸ However, in our study, cGAS was not correlated with STING, suggesting that the positive correlation between ATRX and STING is independent of cGAS in GBM. In addition, the polycomb-group protein EZH2 has been previously demonstrated to promote RAD51-mediated HRR via H3K27me3 to enhance the proliferation of glioma,¹⁹ therefore, the close correlation among γ H2AX, RAD51, and H3K27me3 identified in our study supports their oncogenic regulations from clinical perspectives. Further integrated analysis showed that the positive regulation between ATRX and STING was exclusive to tissues with ATRX^{wt}/IDH1^{wt} (Figure 3c, $p = 0.0089$). Taken together, our data support the idea that ATR and STING positively regulating each other independent of cGAS is exclusive to GBM patients.

Next, a LASSO risk-scoring model predictive of relapse based on the expression of ATRX and STING in the discovery cohort was successfully established with the coefficients of -0.045194 and 0.037555 for ATRX and STING, respectively. The ROC curve showed that the risk scores significantly predicted the relapse with an AUC of 0.686 (Figure 3d, $p = 0.0071$). Moreover, results from univariate and multivariate Cox

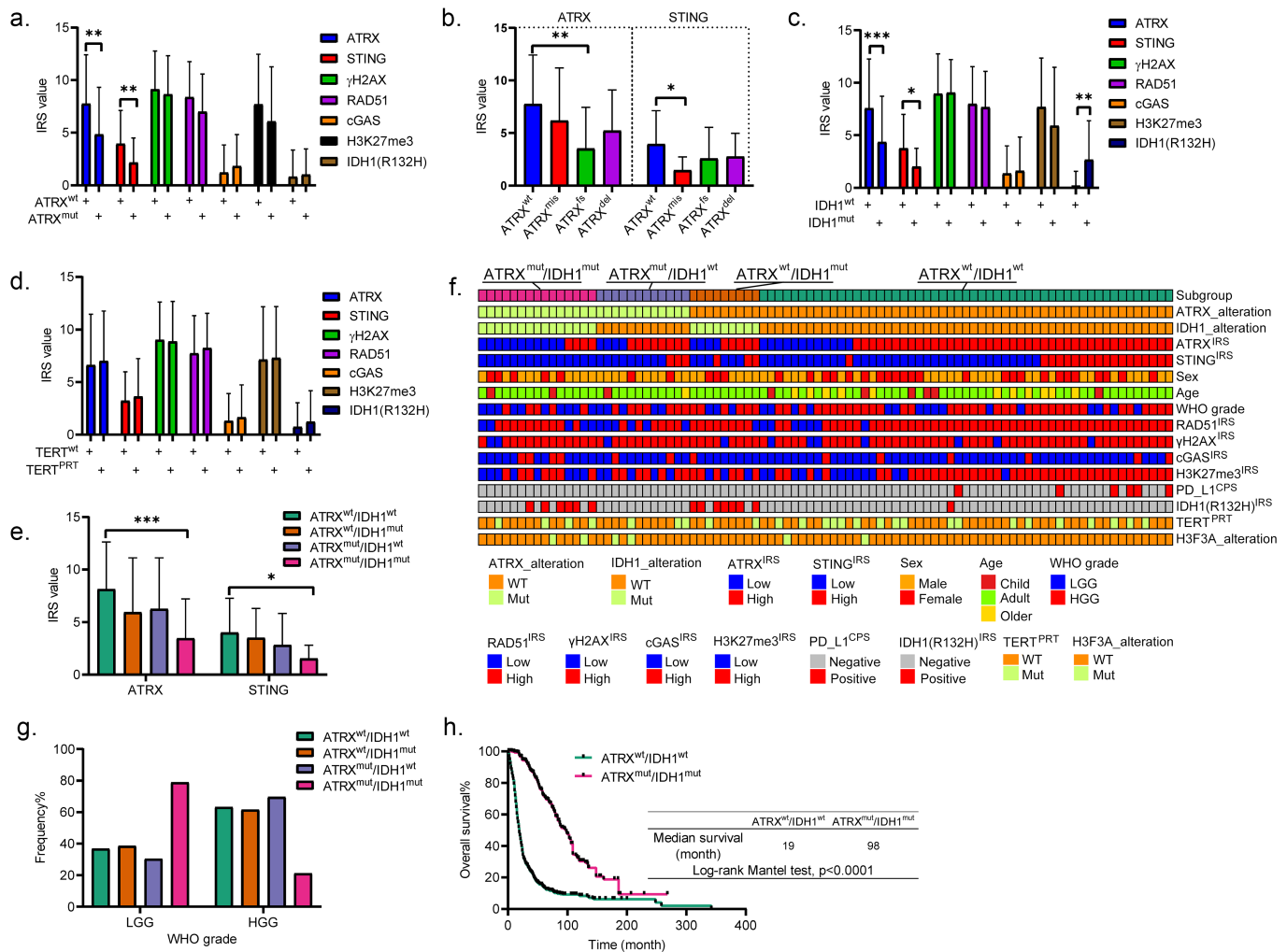


Figure 2. ATRX and STING are both highly expressed in HGG with wild-type ATRX and IDH1. (a). The bar plots showing the different expression of indicated proteins in tissues with ATRX^{wt} or ATRX^{mut}. The IRS values are shown as mean \pm STD. $**p < 0.01$. (b). The bar plots showing the different expression of ATRX and STING in tissues with different types of ATRX mutations. mis, missense; fs, frameshift; del, deletion. The IRS values are shown as mean \pm STD. $*p < 0.05$, $**p < 0.01$. (c). The bar plots showing the different expression of indicated proteins in tissues with IDH1^{wt} or IDH1^{mut}. The IRS values are shown as mean \pm STD. $*p < 0.05$, $**p < 0.01$, $***p < 0.001$. (d). The bar plots showing the different expression of indicated proteins in glioma tissues with TERT^{wt} or TERT^{prt}. The IRS values are shown as mean \pm STD. (e). The bar plots showing the different expression of ATRX and STING in ATRX and IDH1 genetically stratified glioma subgroups. The IRS values are shown as mean \pm STD. $*p < 0.05$, $**p < 0.01$, $***p < 0.001$. (f). The heatmaps showing the features of clinicopathology, genetic alterations, immune proteins, and HRR proteins in ATRX and IDH1 genetically stratified glioma subgroups. (g). The bar plots showing the frequency of ATRX and IDH1 genetically stratified cases in LGG and HGG. (h). The KM survival curves showing the different OS rates between glioma patients from cBioportal database with ATRX^{wt}/IDH1^{wt} and ATRX^{mut}/IDH1^{mut}.

regression analysis revealed that the WHO grade and the risk score were two independent prognostic markers for glioma patients (Figure 3e, $p < 0.0001$ for WHO grade, $p = 0.039$ for risk score), as validated by the KM survival curve that the 5-year OS rate of glioma patients with high risk was significantly lower than those with low risk (Figure 3f, 15% vs 55%, $HR_{high/low} = 2.610$, 95% CI: 1.197 to 5.694, $p = 0.006$).

Additionally, two glioma cohorts from CGGA with recurrence status (CGGA_325 and CGGA_693) were used to externally validate the above findings. As shown in Figure S2A, the ROC curve showed that the risk scores based on the expression of ATRX and STING from CGGA_325 significantly predicted the recurrence with an AUC of 0.5789 ($p = 0.027$). And the median survival time of patients with high risk was significantly shorter than those with low risk (Figure S2B, 15 months vs 40 months, $HR_{high/low} = 2.079$, 95% CI: 1.504 to 2.875, $p < 0.0001$). Similarly, the scores from CGGA_693 also significantly predicted the recurrence with an AUC of 0.6028

(Figure S2C, $p < 0.0001$). And the median survival time of patients with high risk was significantly shorter than those with low risk (Figure S2D, 28 months vs 60 months, $HR_{high/low} = 1.398$, 95% CI: 1.142 to 1.712, $p = 0.0017$). Overall, our findings highlight that the high expression of ATRX and STING is closely correlated to drive the recurrence in GBM, thus leading to poorer survival for these patients.

STING targeted therapies are promising in HGG cells independent of STING levels and STING pathway activation

For the sake of precision therapies, we further analyzed the differential prognosis of the above risk scores in clinicopathological and molecular stratified subgroups. As shown in Figure 4a, the risk scores showed different prognosis in RAD51, ATRX, TERT alteration, and IDH1 alteration stratified subgroups. However, the interacted p-values between the risk scores and

Table 1. Characteristics of clinicopathology, genetic alterations, immune, and DDR proteins in ATRX and IDH1 genomically stratified subgroups in the overall cohort.

	ATRX ^{wt} /IDH1 ^{wt}	ATRX ^{wt} /IDH1 ^{mut}	ATRX ^{mut} /IDH1 ^{wt}	ATRX ^{mut} /IDH1 ^{mut}	χ ² test pval
Total N (%)	68 (54.0%)	14 (11.1%)	22 (17.5%)	22 (17.5%)	
Sex	68 (100.0%)	14 (100.0%)	22 (100.0%)	22 (100.0%)	
Male	41 (60.3%)	8 (57.1%)	14 (63.6%)	15 (68.2%)	
Female	27 (39.7%)	6 (42.9%)	8 (36.4%)	7 (31.8%)	0.895
Age	68 (100.0%)	14 (100.0%)	22 (100.0%)	22 (100.0%)	
Child	7 (10.3%)	0 (0.0%)	2 (9.1%)	2 (9.1%)	
Adult	48 (70.6%)	13 (92.9%)	16 (72.7%)	19 (86.4%)	
Older	13 (19.1%)	1 (7.1%)	4 (18.2%)	1 (4.5%)	0.467
WHO stage	68 (100.0%)	14 (100.0%)	22 (100.0%)	22 (100.0%)	
LGG	25 (36.8%)	5 (35.7%)	7 (31.8%)	16 (72.7%)	
HGG	43 (63.2%)	9 (64.3%)	15 (68.2%)	6 (27.3%)	0.015
γH2AX ^{IRS}	62 (91.2%)	11 (78.6%)	18 (81.8%)	18 (81.8%)	
Low	10 (16.1%)	1 (9.1%)	2 (11.1%)	2 (11.1%)	
High	52 (83.9%)	10 (90.9%)	16 (88.9%)	16 (88.9%)	0.871
RAD51 ^{IRS}	68 (100.0%)	14 (100.0%)	21 (95.5%)	22 (100.0%)	
Low	12 (17.6%)	3 (21.4%)	6 (28.6%)	8 (36.4%)	
High	56 (82.4%)	11 (78.6%)	15 (71.4%)	14 (63.6%)	0.298
ATRX ^{IRS}	68 (100.0%)	14 (100.0%)	21 (95.5%)	22 (100.0%)	
Low	17 (25.0%)	7 (50.0%)	9 (42.9%)	16 (72.7%)	
High	51 (75.0%)	7 (50.0%)	12 (57.1%)	6 (27.3%)	0.001
cGAS ^{IRS}	60 (88.2%)	9 (64.3%)	16 (72.7%)	18 (81.8%)	
Low	54 (90.0%)	8 (88.9%)	14 (87.5%)	14 (77.8%)	
High	6 (10.0%)	1 (11.1%)	2 (12.5%)	4 (22.2%)	0.594
STING ^{IRS}	57 (83.8%)	10 (71.4%)	16 (72.7%)	17 (77.3%)	
Low	38 (66.7%)	7 (70.0%)	13 (81.3%)	17 (100.0%)	
High	19 (33.3%)	3 (30.0%)	3 (18.8%)	0 (0.0%)	0.041
PD-L1 ^{CPS}	56 (82.4%)	9 (64.3%)	15 (68.2%)	18 (81.8%)	
Negative	50 (89.3%)	9 (100.0%)	15 (100.0%)	18 (100.0%)	
Positive	6 (10.7%)	0 (0.0%)	0 (0.0%)	0 (0.0%)	0.188
H3K27me3 ^{IRS}	59 (86.8%)	10 (71.4%)	17 (77.3%)	19 (86.4%)	
Low	17 (28.8%)	4 (40.0%)	7 (41.2%)	11 (57.9%)	
High	42 (71.2%)	6 (60.0%)	10 (58.8%)	8 (42.1%)	0.144
IDH1(R132H) ^{IRS}	62 (91.2%)	10 (71.4%)	17 (77.3%)	20 (90.9%)	
Negative	61 (98.4%)	3 (30.0%)	16 (94.1%)	11 (55.0%)	
Positive	1 (1.6%)	7 (70.0%)	1 (5.9%)	9 (45.0%)	<0.0001
TERT ^{PRT}	68 (100.0%)	14 (100.0%)	22 (100.0%)	22 (100.0%)	
WT	48 (70.6%)	9 (64.3%)	13 (59.1%)	17 (77.3%)	
Mut	20 (29.4%)	5 (35.7%)	9 (40.9%)	5 (22.7%)	0.585
H3F3A	68 (100.0%)	14 (100.0%)	22 (100.0%)	22 (100.0%)	
WT	65 (95.6%)	14 (100.0%)	19 (86.4%)	20 (90.9%)	
Mut	3 (4.4%)	0 (0.0%)	3 (13.6%)	2 (9.1%)	0.305

pval, p-value; LGG, lower-grade glioma; HGG, higher-grade glioma; IRS, immunoreactive score; WT, wild-type; Mut, mutated; PRT, promoter; DDR, DNA damage repair.

above factors revealed that the scores independently predicted the survival for glioma patients characterized with high expression of RAD51 ($p = 0.004$) and TERT^{wt} ($p = 0.004$). Of note, the risk scores were significantly higher in HGG tissues ($p = 0.028$) and in tissues with a high expression of STING ($p < 0.0001$), which was further supported by data from CGGA_325 (Figure S2E, $p < 0.0001$) and CGGA_693 (Figure S2F, $p < 0.0001$). Accordingly, we speculate that DDR inhibitors and STING-related therapies might be promising in treating HGG patients with high risks of recurrence.

By examining the basic expression of STING in a panel of HGG cells (Figure 4b), we divided them into high expression models (STING^{high}) (H4, A172, and SW1783) and low expression models (STING^{low}) (U87, U251, LN229, and TJ905) for following therapeutic explorations. Firstly, we investigated the responses of STING^{high} and STING^{low} cells to STING agonist diABZI, which has a half maximal effective concentration (EC₅₀) of 130 nM for human STING,²⁰ and STING inhibitor SN-011, which competes with cyclic dinucleotide for the binding pocket of the STING dimer to block its activation with an IC₅₀ of 76 nM.²¹ Results from cell viability assays showed that the STING^{high} cells tended to be more sensitive to diABZI than

STING^{low} cells (Figure 4c). However, data from colony formation assays (CFAs) revealed that the diABZI significantly inhibited the growth of both STING^{high} (H4) and STING^{low} (U87) cells (Figure 4d, $p = 0.0158$ for vehicle vs 1 μM and $p = 0.0019$ for vehicle vs 5 μM in H4 cells, while $p = 0.0395$ for vehicle vs 1 μM and $p = 0.0141$ for vehicle vs 5 μM in U87 cells), suggesting that the diABZI is an effective anti-cancer drug for HGG patients regardless of STING levels. More interestingly, although there was no difference in the responses of STING^{high} and STING^{low} cells to SN-011 (Figure 4e), data from CFAs demonstrated that SN-011 also significantly suppressed the growth of STING^{high} and STING^{low} cells (Figure 4f, $p = 0.0405$ for H4 cells and $p = 0.0051$ for U87 cells). Overall, we believe that STING targeted therapies are possibly promising in suppressing the growth of HGG cells independent of STING levels.

Furthermore, we detected the STING pathway activation related inflammatory genes using qRT-PCR assays, including *TBK1*, *LKB1*, *IRF3*, *CXCL10*, *IFNβ1*, *TRAF3*, *NF-κB*, *IFIT3*, and *IL-6*, and its activation-related proteins, phosphorylated STING (pSTING and S366) and TBK1 (pTBK1 and S172), using western blotting assays,²² in response to STING targeted treatments. Data

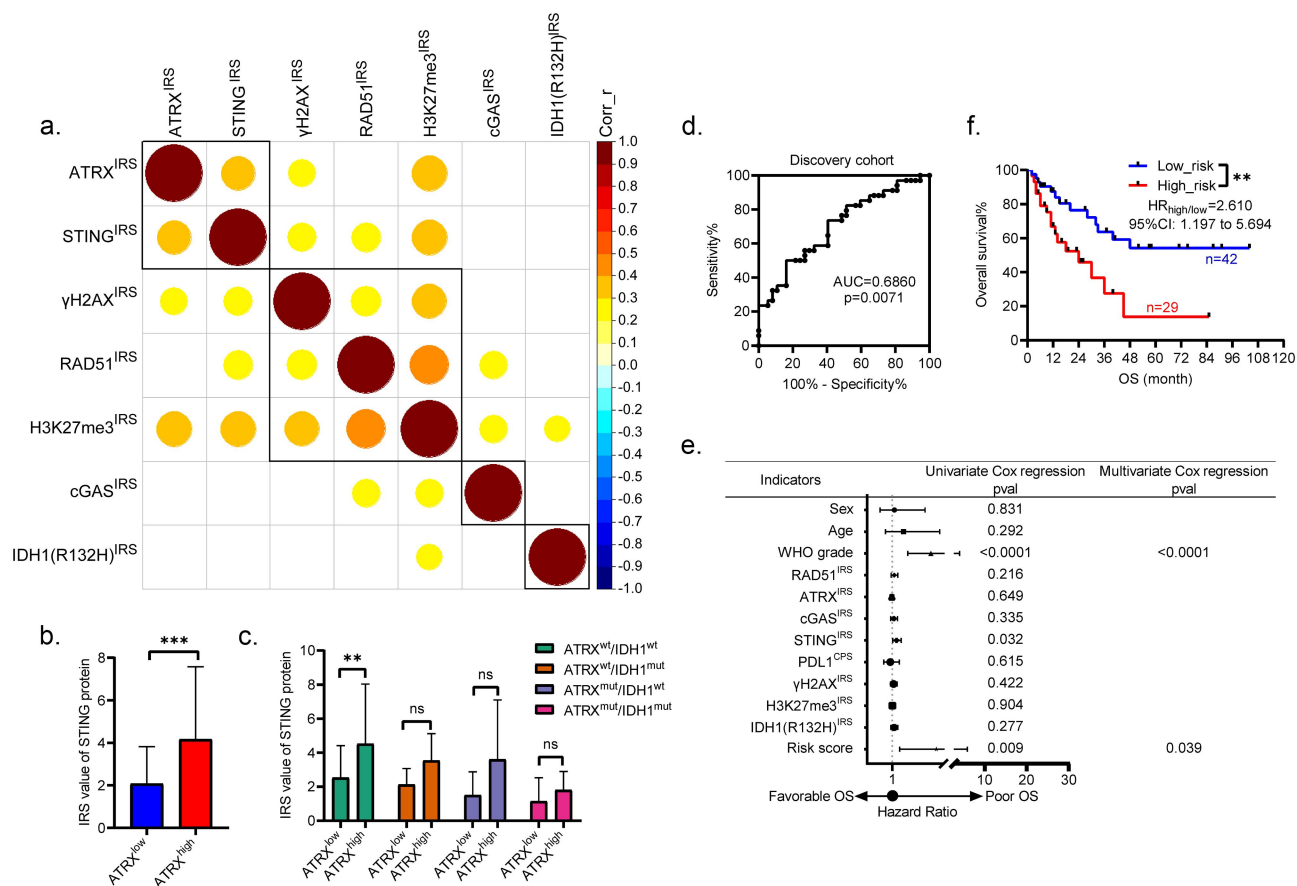


Figure 3. ATRX is positively correlated with STING to drive the relapse of HGG with wild-type ATRX and IDH1. (a). The matrix showing the mutual correlations among indicated proteins in the overall cohort. Blank grids mean $p > 0.05$, while colored grids mean $p < 0.05$. Corr_r, correlation coefficient. (b). The bar plots showing the different expression of STING in tissues with ATRX^{low} or ATRX^{high}. The IRS values are shown as mean \pm STD. *** $p < 0.001$. (c). The bar plots showing the differential expression of STING in ATRX and IDH1 genomically stratified subgroups with ATRX^{high} and ATRX^{low}. The IRS values are shown as mean \pm STD. ** $p < 0.01$. (d). The ROC curve evaluating the predictive capability of relapse risk scores in the discovery cohort. AUC = 0.6860, ** $p < 0.01$. (e). The forest plot showing the univariate and multivariate cox regression analysis used to identify independent prognostic markers in the discovery cohort. (f). The KM survival curves showing the different OS rates between patients with low_risk and high_risk scores in the discovery cohort. ** $p < 0.01$.

from qRT-PCR assays showed that the STING agonist diABZI dramatically induced upregulation of all the inflammatory genes in H4 cells (Figure 5a, * $p < 0.05$, ** $p < 0.01$, *** $p < 0.001$ and **** $p < 0.0001$), whereas the STING inhibitor SN-011 not only down-regulated *IFIT3*, but also upregulated *IFNB1* and *TRAF3* in H4 cells (Figure 5b, * $p < 0.05$, ** $p < 0.01$, *** $p < 0.001$). However, data from western blotting assays showed that the STING agonist obviously induced the activation of STING pathway by reducing the expression of STING, rather than affecting ATRX and cGAS levels, in STING proficient H4 and A172 cells (Figure 5c,d, $p = 0.013$ for STING, $p = 0.009$ for pSTING, and $p < 0.0001$ for pTBK1 in H4 cells, $p = 0.024$ for STING, $p = 0.003$ for pSTING, and $p = 0.024$ for pTBK1 in A172 cells), whereas the SN-011 had no obvious effects on the STING pathway activation due to the low activation of STING pathway in these cells (Figure 5e,f).

Unexpectedly, the diABZI and SN-011 both significantly induced upregulation of STING pathway related inflammatory genes in STING deficient U87 cells, including *IRF3*, *TRAF3*, *NF- κ B*, *IFIT3*, and *IL-6* in response to diABZI (Figure 5g, * $p < 0.05$, ** $p < 0.01$, *** $p < 0.001$), and *TBK1*, *TRAF3*, *NF- κ B*, and *IL-6* in response to SN-011 (Figure 5h, * $p < 0.05$, ** $p < 0.01$, **** $p < 0.0001$). However, results from western blotting assays showed

that the STING pathway, ATRX and cGAS levels were not all significantly affected by these treatments (Figure 5i,j). Taken above all, we believe that STING targeted therapies are possibly promising in suppressing the growth of HGG cells independent of STING levels and STING pathway activation. In addition, ATRX possibly acts as an upstream regulator for STING independent of cGAS in HGG cells. Further mechanistic studies will help warrant our hypothesis in the future.

RAD51 inhibitor B02 exclusively sensitizes HGG cells with high expression of STING to temozolomide *in vitro* and *in vivo*

Next, we explored the potential therapies of DDR inhibitors in STING^{high} and STING^{low} HGG cells, including PARPi Olaparib, ATRi AZD6738 (AZD), RAD51i B02, and TMZ. Interestingly, data from cell viability assays revealed that the STING^{high} cells were more resistant to TMZ than STING^{low} cells (Figure S3A, $p = 0.029$), while there was no significant difference in the responses to other DDR inhibitors used as monotherapies (Figure S3B-D).

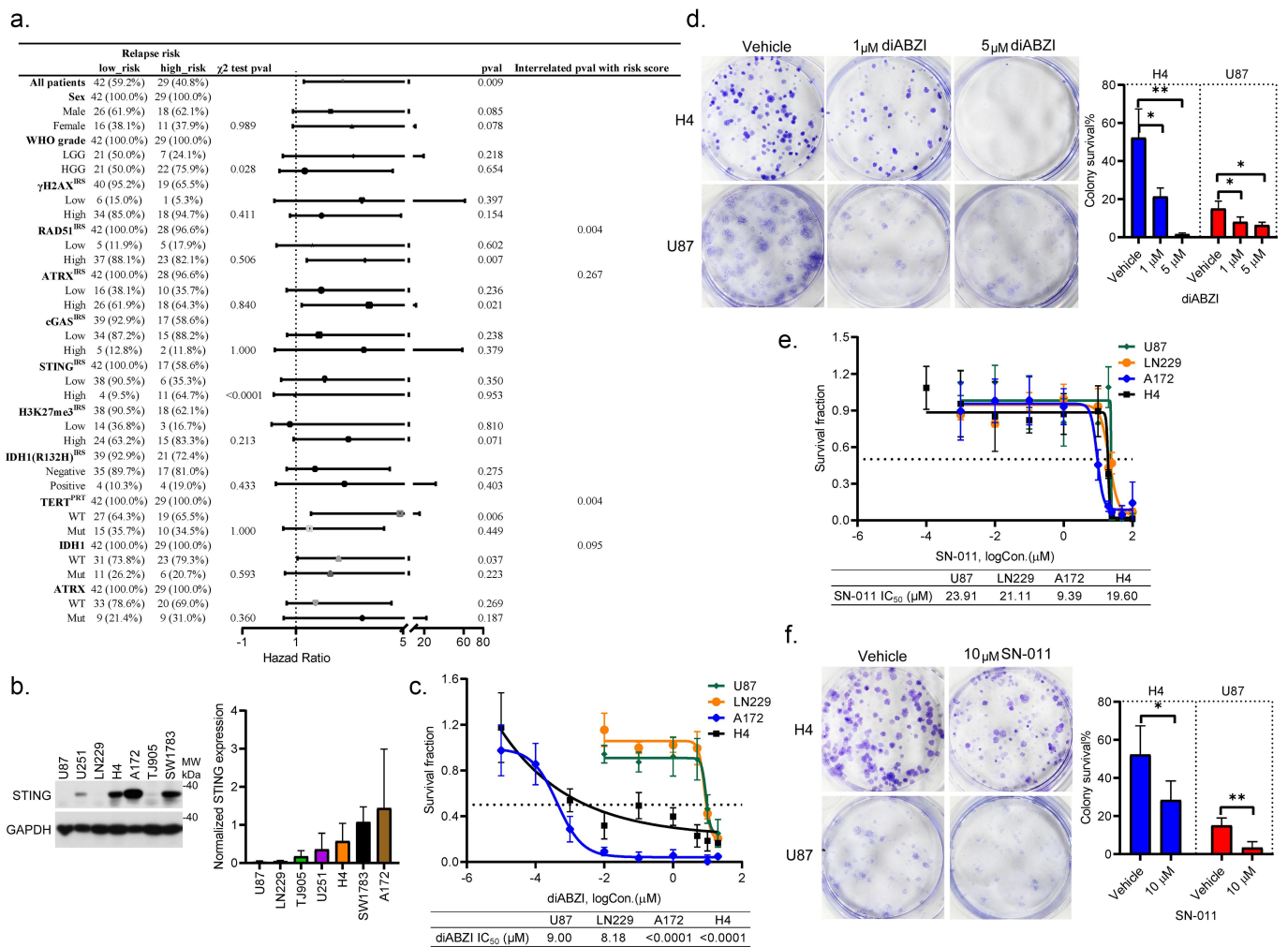


Figure 4. The STING targeted therapies are both promising in suppressing the growth of HGG cells regardless of STING levels. (a). The multiplex forest plot showing the correlation and differential prognosis of risk scores in clinical and molecular features stratified subgroups. (b). The representative western blotting results showing the expression of indicated proteins in HGG cells (left panel). The GAPDH normalized relative expression of STING from at least three independent experiments is shown as mean \pm STD (right panel). (c). The survival curves showing the responses of indicated HGG cells to STING agonist diABZI. Data from at least three independent assays are shown as mean \pm STD. (d). The representative colony formation results of indicated HGG cells in response to different concentrations of diABZI, taking the vehicle treated cells as controls. Data from three independent experiments are shown as mean \pm STD. * p < 0.05. ** p < 0.01. (e). The survival curves showing the responses of indicated HGG cells to STING inhibitor SN-011. Data from at least three independent assays are shown as mean \pm STD. (f). The representative colony formation results of indicated HGG cells in response to SN-011, taking the vehicle treated cells as controls. Data from three independent experiments are shown as mean \pm STD. * p < 0.05, ** p < 0.01.

Then, triggered by the above clinical findings that the relapse risk scores specifically predicted the survivals for HGG patients with high expression of RAD51, we further investigated the combined therapeutic effects of B02 and TMZ. Surprisingly, cell viability results showed that the RAD51i B02 significantly sensitized the STING^{high} HGG cells to the TMZ treatment (Figure 6a–c), while it exhibited few effects on the STING^{low} HGG cells (Figure 6d,e). Moreover, data from CFAs confirmed that the combined therapeutic effects of B02 and TMZ were exclusive to STING^{high} cells (Figure 6f,g, p = 0.0158), while the STING^{low} cells (U87 and LN229) were dramatically sensitive to TMZ (Figure 6h–k, p < 0.0001), consistent with the above cell viability results. Then, we further performed the *in vivo* therapeutic study using NOD SCID mice subcutaneously planted with LN229 (STING^{low}) or H4 (STING^{high}) cells, respectively. Most excitingly, although TMZ and TMZ plus B02 significantly inhibited the growth of H4 cells (Figure 7a,b, p = 0.0025 for TMZ vs Vehicle, while p < 0.0001 for

TMZ plus B02 vs Vehicle), TMZ plus B02 showed a more obvious inhibitory activity than TMZ (Figure 7a,b, p = 0.0248 for TMZ vs TMZ plus B02). In addition, all the above results were further supported by the weights of xenografts resected at the end of the study (Figure 7c, p = 0.0445 for Vehicle vs. TMZ, p = 0.0004 for Vehicle vs. TMZ plus B02, while p = 0.0473 for TMZ vs TMZ plus B02). However, the growth (Figure 7d,e) and tumor weights (Figure 7f) of LN229 cells were not statistically different among Vehicle, TMZ, and TMZ plus B02 groups. Of note, both TMZ and TMZ plus B02 were not toxic to the mice, supported by their stable body weights (Figure 7g,h). Taken together, we propose that STING levels will help guide a novel therapeutic strategy to treat patients diagnosed with ATRX^{wt}/IDH1^{wt} HGG. However, further studies elucidating the complex regulatory loops among ATRX, STING, and RAD51 will help warrant a more precise manipulation of the novel combined therapy in treating specific subgroups of aggressive gliomas.

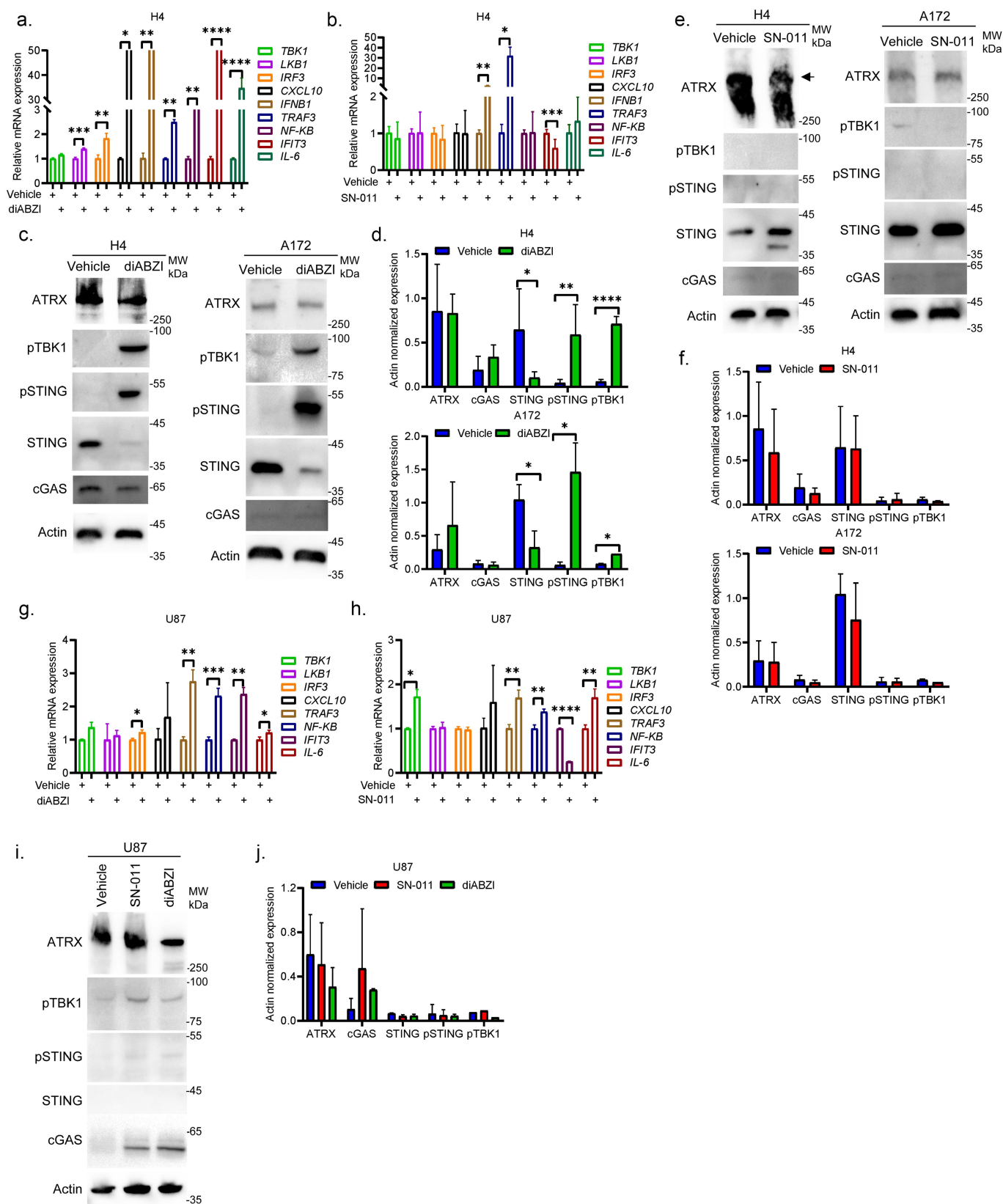


Figure 5. The STING targeted therapies are both promising in suppressing the growth of HGG cells regardless of STING pathway activation. (a–b). The bar plots showing the differential expressions of STING-related inflammatory genes in H4 cells tested by qRT-PCR assays in response to diABZI (a) and SN-011 (b). Data from three independent experiments are shown as mean \pm STD. * p < 0.05, ** p < 0.01, *** p < 0.001, **** p < 0.0001. (c,d). The representative western blotting results of indicated proteins in H4 and A172 cells treated with vehicle or diABZI (c). The actin normalized expression of indicated proteins from at least three independent assays are shown as mean \pm STD (d). * p < 0.05, ** p < 0.01 and **** p < 0.0001. (e,f). The representative western blotting results of indicated proteins in H4 and A172 cells treated with vehicle or SN-011 (e). The actin normalized expression of indicated proteins from at least three independent assays are shown as mean \pm STD (f). (g,h). The bar plots showing the differential expressions of STING related inflammatory genes in U87 cells tested by qRT-PCR assays in response to diABZI (g) and SN-011 (h). Data from three independent experiments are shown as mean \pm STD. * p < 0.05, ** p < 0.01, *** p < 0.001, and **** p < 0.0001. (i,j). The representative western blotting results of indicated proteins in U87 cells treated with vehicle or diABZI or SN-011 (i). The actin normalized expression of indicated proteins from at least three independent assays are shown as mean \pm STD.

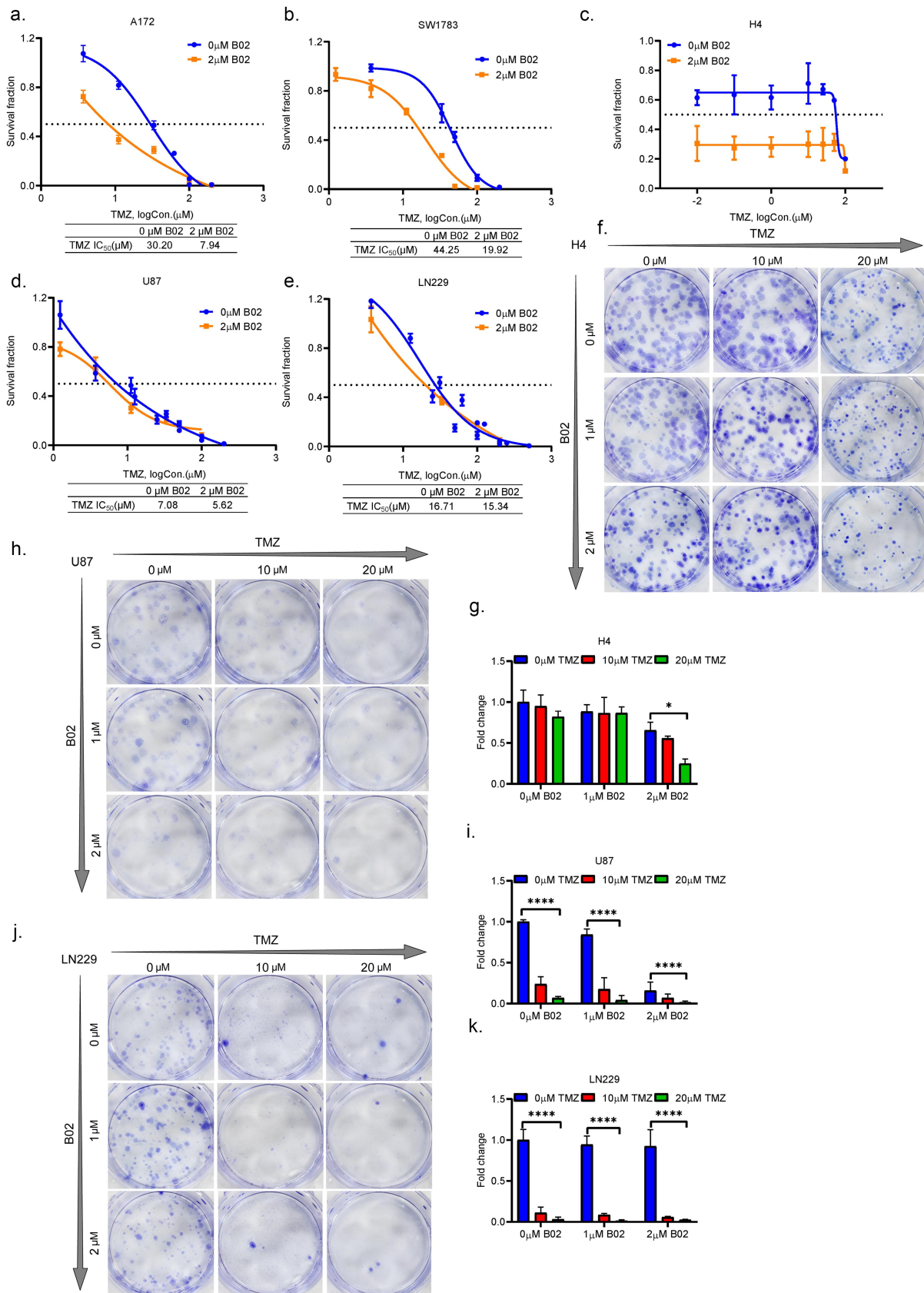


Figure 6. RAD51 inhibitor B02 significantly sensitizes HGG cells with high expression of STING to TMZ *in vitro*. (a–c). The survival curves showing the responses of STING proficient A172 (a), SW1783 (b) and H4 (c) cells to TMZ treatments with or without 2 μM RAD51 inhibitor B02. Data from at least three independent experiments are shown as mean \pm STD. (d–e). The survival curves showing the responses of STING deficient U87 (d) and LN229 (e) cells to TMZ treatments with or without 2 μM RAD51 inhibitor B02. Data from at least three independent experiments are shown as mean \pm STD. (f–k). The representative colony formation results of H4 cells (f), U87 cells (h) and LN229 cells (j) in response to different combined treatments of B02 and TMZ. The vehicle treated cells (0 μM B02 + 0 μM TMZ) normalized fold changes of H4 cells (g), U87 cells (i) and LN229 cells (k) from three independent experiments are shown as mean \pm STD (g). * $p < 0.05$.

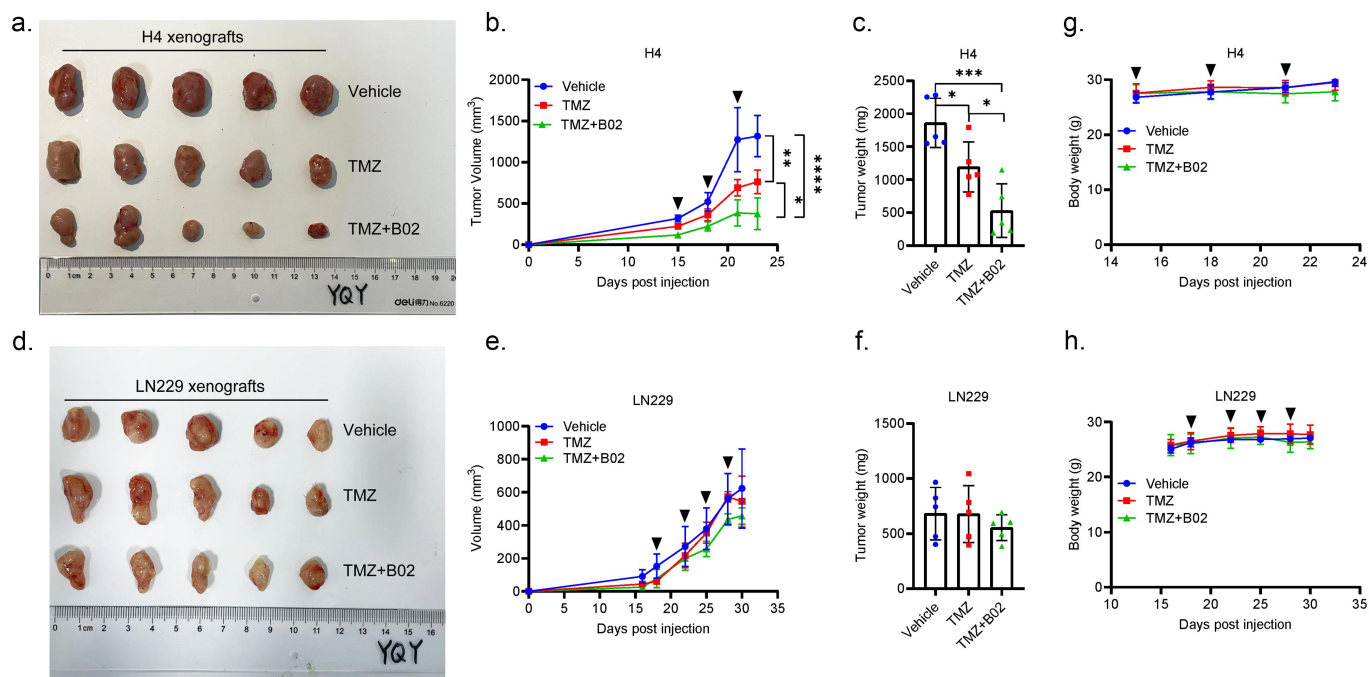


Figure 7. B02 exclusively sensitizes HGG cells with high expression of STING to TMZ *in vivo*. (a). Image of H4 (STING^{high}) xenografts from NOD SCID mice administered with vehicle ($n = 5$), 50 mg/kg TMZ ($n = 5$) and 50 mg/kg TMZ plus 25 mg/kg B02 ($n = 5$), respectively. (b). The growth curves of H4 xenografts in response to indicated treatments, shown by the tumor volumes (mm^3). (c). The tumor weights of H4 xenografts in figure 7A. (d). Image of LN229 (STING^{low}) xenografts from NOD SCID mice administered with vehicle ($n = 5$), 50 mg/kg TMZ ($n = 5$) and 50 mg/kg TMZ plus 25 mg/kg B02 ($n = 5$), respectively. (e). The growth curves of LN229 xenografts in response to indicated treatments, shown by the tumor volumes (mm^3). (f). The tumor weights of LN229 xenografts in figure 7D. (g–h). The body weights of H4 (g) and LN229 (h) bearing NOD SCID mice in response to indicated treatments. Black arrows indicate the therapeutic administration. * $p < 0.05$, ** $p < 0.01$, *** $p < 0.001$, **** $p < 0.0001$.

Discussion

In summary, our integrated study highlights a non-canonical role of STING in gliomagenesis that is different from its well-documented function in tumor immunosurveillance.²³ Expressions of ATRX and STING are significantly higher and closely correlated with each other in a positive manner in HGG characterized with ATRX^{wt}/IDH1^{wt}, which is classified as ATRX^{retained}/IDH^{wt} GBM.² Moreover, the relapse risk scores based on the expression of ATRX and STING at both transcriptional and translational levels specifically predict poor survivals for HGG patients, characterized by high expression of HRR protein RAD51 as well as STING. Guided by these clinical findings, our therapeutic studies highlight that RAD51 inhibitor B02 specifically sensitizes HGG cells with high expression of STING to TMZ treatments, while the STING targeted strategies are promising in treating HGG cells regardless of STING levels and STING pathway activation.

Enormous studies have confirmed an overlap of somatic mutations between ATRX and IDH in glioma,¹⁶ which accounts for 17.5% in our overall cohort (Table 1). ATRX^{mut} is known to cause its protein loss,¹⁶ a deficiency of which has been reported to reduce the adaptive immune responses by downregulating the cGAS-STING signaling to increase sensitivity of sarcoma cells to TVEC, an oncolytic herpes virus that is currently FDA approved for the treatment of aggressive melanomas.¹⁸ In glioma, we found that the expression of STING is significantly reduced in ATRX^{mut} tissues, specifically those with ATRX^{mis} mutations. Besides, its expression is also

downregulated in IDH1^{mut} tissues, but not in tissues with TERT^{PRT}. Further integrated analysis showed that, similar to ATRX, its high expression is exclusive to GBM patients. Previous studies have also supported our above findings that STING, tested by IHC staining, is highest in GBM tissues than other glioma types, including normal brain tissues.²⁴ Their therapeutic studies with GBM explants have shown that the STING agonist ADU-S100 significantly increases the STING pathway related immune responses, shown to be inflammatory macrophages, neutrophils, and natural killer populations.²⁴ However, our data showed that both STING inhibitor SN-011 and STING agonist diABZI significantly inhibit the growth of STING deficient and proficient HGG cells, although cells with high expression of STING seem to be more sensitive to diABZI treatments. Mechanistically, SN-011 and diABZI both obviously induce upregulation of STING pathway related inflammatory genes in HGG cells, regardless of whether the STING pathway is activated. It seems that the STING targeted therapies in HGG cells are more complex than we have imagined. Further preclinical studies are required to deeply uncover their underlying mechanisms before putting them into clinical practice.

It is known that most of the lethal anti-cancer agents are ineffective in treating aggressive GBMs due to the existence of blood–brain barrier. According to our results from CFAs, we see that the diABZI effectively suppresses the growth of GBM cells at much lower concentrations than SN-011; therefore, we think that the diABZI is a more appropriate STING targeted therapy for GBM patients. Of note, our western blotting data also suggest that the diABZI significantly induces the activation

of the STING pathway by downregulating the expression of STING, which is in line with findings from other teams.²⁵ Therefore, it will be beneficial to elucidate its underlying mechanisms to guide a more precise design of STING agonists in the future.

Clinically, multiple DDRi chemotherapies have been investigated to remodel the TIME by activating STING-inflammatory signaling, thus improving the efficacy of cancer immunotherapy. For instance, the PARP inhibitors including niraparib, olaparib, rucaparib, and ATR inhibitors including M6620, AZD6738, BAY1895344 have been widely used to facilitate the PD-1/PD-L1/CTLA-4 targeted immunotherapeutic responses in multiple solid tumors.⁷ In this study, our data demonstrate that the responses of HGG cells with low and high expression of STING are not significantly different from PARPi, ATRi, and RAD51i when they are used as monotherapies. Guided by the differential prognosis of relapse risk scores in glioma patients with high expression of RAD51, we found that RAD51i B02 specifically sensitizes STING proficient HGG cells to TMZ treatment *in vitro* and *in vivo*, providing a STING-guided combined therapy for specific subgroups in HGG. Further mechanistic studies uncovering the direct relationships among ATRX, STING, and RAD51 will help ensure appropriate translations of the above phenotype findings in precise diagnosis and treatment of gliomas, specifically the aggressive GBM.

Although a non-canonical role of STING, positively correlated with ATRX in driving the relapse of GBM, has been uncovered from clinical perspectives, there are still some limitations in our study. Firstly, the sample size of the discovery cohort used to construct the relapse predictive risk-scoring model is relatively small, a larger cohort is required to further warrant its predictive reliability. Secondly, this is a single-center retrospective study, where clinically registered prospective studies from multi-centers will help to ensure the clinical translation of the relapse predictive model. Thirdly, further mechanistic studies elucidating the direct regulations among ATRX, RAD51, and STING are still required to ensure the precise manipulation of the STING-guided therapy in treating GBM with high relapse risk. In summary, our findings in this study not only highlight that ATRX is closely correlated with STING to drive the relapse of HGG, but also provide a STING-guided combined strategy to treat these patients. Translation of these findings will ultimately improve the outcomes for ATRX and IDH1 genomically stratified subgroups in HGG.

Acknowledgments

We deeply appreciate Professor Yong, Ren from the Department of Pathology, Wuhan Central Theater Command General Hospital, for collecting glioma tissue blocks and clinicopathological information. Besides, we also sincerely thank the executive director Dr. Tianhai, Ji in our department for moral support and encouragement at all times. This study was financially supported by the funds from Shanghai Ninth People's Hospital, Shanghai Jiao Tong University School of Medicine (JYZZ195, YJXKB2020013).

Disclosure statement

No potential conflict of interest was reported by the author(s).

Funding

The work was supported by the Shanghai Ninth People's Hospital, Shanghai Jiao Tong University School of Medicine [JYZZ195].

ORCID

Qingyuan Yang  <http://orcid.org/0000-0001-8808-1113>

Authors' contributions

Conception and Funding: Q.Y.; **Data collection:** Q.Y., M.Z.; M.L.; S.J.; C.H.; **Data Analysis:** Q.Y.; M.Z.; M.L.; **Writing:** Q.Y.; **Review and final approval:** All authors.

Availability of data and materials

All the datasets are presented in the main manuscript or additional supporting files wherever possible. The targeted NGS data were deposited in the National Genomics Data Center under the accession number PRJCA012429.

References

- Bauchet L, Ostrom QT. Epidemiology and molecular epidemiology. *Neurosurg Clin N Am.* 2019 Jan;30(1):1–16. doi:10.1016/j.nec.2018.08.010.
- Berger TR, Wen PY, Lang-Orsini M, Chukwueke UN. World health organization 2021 classification of central nervous system tumors and implications for therapy for adult-type gliomas: a review. *JAMA Oncol.* Oct 1 2022;8(10):1493–1501. doi:10.1001/jamaoncol.2022.2844.
- Gallego O. Nonsurgical treatment of recurrent glioblastoma. *Curr Oncol.* 2015 Aug;22(4):273–281. doi:10.3747/co.22.2436.
- Kannan S, Murugan AK, Balasubramanian S, Munirajan AK, Alzahrani AS. Gliomas: genetic alterations, mechanisms of metastasis, recurrence, drug resistance, and recent trends in molecular therapeutic options. *Biochem Pharmacol.* 2022 Jul;201:115090. doi:10.1016/j.bcp.2022.115090.
- Haase S, Banerjee K, Mujeeb AA, Hartlage CS, Núñez FM, Núñez FJ, Alghamri MS, Kadiyala P, Carney S, Barissi MN. et al. H3.3-G34 mutations impair DNA repair and promote cGAS/STING-mediated immune responses in pediatric high-grade glioma models. *J Clin Invest.* Nov 15 2022;132(22). doi:10.1172/JCI154229.
- Pang Y, Chen X, Ji T, Cheng M, Wang R, Zhang C, Liu M, Zhang J, Zhong C. The chromatin remodeler ATRX: role and mechanism in biology and cancer. *Cancers Basel.* Apr 10 2023;15(8):2228. doi:10.3390/cancers15082228.
- Reislander T, Groelly FJ, Tarsounas M. DNA damage and cancer immunotherapy: a STING in the tale. *Mol Cell.* Oct 1 2020;80(1):21–28. doi:10.1016/j.molcel.2020.07.026.
- Fedchenko N, Reifenrath J. Different approaches for interpretation and reporting of immunohistochemistry analysis results in the bone tissue – a review. *Diagn Pathol.* Nov 29 2014;9(1):221. doi:10.1186/s13000-014-0221-9.
- Kulangara K, Hanks DA, Waldroup S, Peltz L, Shah S, Roach C, Juco JW, Emancipator K, Stanforth D. Development of the combined positive score (CPS) for the evaluation of PD-L1 in solid tumors with the immunohistochemistry assay PD-L1 IHC 22C3 pharmDx. *J Clin Oncol.* 2017;35(15_suppl):e14589–e14589. doi:10.1200/JCO.2017.35.15_suppl.e14589.
- Gao J, Aksoy BA, Dogrusoz U, Dresdner G, Gross B, Sumer SO, Sun Y, Jacobsen A, Sinha R, Larsson E. et al. Integrative analysis of complex cancer genomics and clinical profiles using the cBioportal. *Sci Signal.* Apr 2 2013;6(269):11. doi:10.1126/scisignal.2004088.
- Zhao Z, Zhang KN, Wang Q, Li G, Zeng F, Zhang Y, Wu F, Chai R, Wang Z, Zhang C. et al. Chinese glioma genome atlas

- (CGGA): a comprehensive resource with functional genomic data from Chinese glioma patients. *Genomics, proteomics & bioinformatics*. 2021 Feb;19(1):1–12. doi:10.1016/j.gpb.2020.10.005.
12. Zhao Z, Meng F, Wang W, Wang Z, Zhang C, Jiang T. Comprehensive RNA-seq transcriptomic profiling in the malignant progression of gliomas. *Sci Data*. Mar 14 2017;4(1):170024. doi:10.1038/sdata.2017.24.
 13. Tentori L, Leonetti C, Scarsella M, d'Amati G, Portarena I, Zupi G, Bonmassar E, Graziani G. Combined treatment with temozolomide and poly(ADP-ribose) polymerase inhibitor enhances survival of mice bearing hematologic malignancy at the central nervous system site. *Blood* Mar. 2002 15; 99(6): 2241–2244. doi:10.1182/blood.V99.6.2241.
 14. Huang F, Mazin AV, Korolev S. A small molecule inhibitor of human RAD51 potentiates breast cancer cell killing by therapeutic agents in mouse xenografts. *PLoS One*. 2014;9(6):e100993. doi:10.1371/journal.pone.0100993.
 15. Nishikawa T, Watanabe R, Kitano Y, Yamamichi A, Motomura K, Ohka F, Aoki K, Hirano M, Kato A, Yamaguchi J. et al. Reliability of IDH1-R132H and ATRX and/or p53 immunohistochemistry for molecular subclassification of grade 2/3 gliomas. *Brain Tumor Pathol*. 2022 Jan;39(1):14–24. doi:10.1007/s10014-021-00418-x.
 16. Liu XY, Gerges N, Korshunov A, Sabha N, Khuong-Quang D-A, Fontebasso AM, Fleming A, Hadjadj D, Schwartzentruber J, Majewski J. et al. Frequent ATRX mutations and loss of expression in adult diffuse astrocytic tumors carrying IDH1/IDH2 and TP53 mutations. *Acta Neuropathol*. 2012 Nov;124(5):615–625. doi:10.1007/s00401-012-1031-3.
 17. Nagtegaal ID, Odze RD, Klimstra D, Paradis V, Rugge M, Schirmacher P, Washington KM, Carneiro F, Cree IA. The 2019 WHO classification of tumours of the digestive system. *Histopathology*. 2020 Jan;76(2):182–188. doi:10.1111/his.13975.
 18. Floyd W, Pierpoint M, Su C, Patel R, Luo L, Deland K, Wisdom AJ, Zhu D, Ma Y, DeWitt SB. et al. Atrx deletion impairs CGAS/STING signaling and increases sarcoma response to radiation and oncolytic herpesvirus. *J Clin Invest*. May 18 2023;133(13):1–17. doi:10.1172/JCI149310.
 19. Yang Q, Nair S, Laknaur A, Ismail N, Diamond MP, Al-Hendy A. The polycomb group protein EZH2 impairs DNA damage repair gene expression in human uterine fibroids. *Biol Reprod*. 2016;94(3):69. doi:10.1095/biolreprod.115.134924.
 20. Ramanjulu JM, Pesiridis GS, Yang J, Concha N, Singhaus R, Zhang S-Y, Tran J-L, Moore P, Lehmann S, Eberl HC. et al. Design of amidobenzimidazole STING receptor agonists with systemic activity. *Nature*. 2018 Dec;564(7736):439–443. doi:10.1038/s41586-018-0705-y.
 21. Hong Z, Mei J, Li C, Bai G, Maimaiti M, Hu H, Yu W, Sun L, Zhang L, Cheng D. et al. STING inhibitors target the cyclic dinucleotide binding pocket. *Proc Natl Acad Sci U S A*. Jun 15 2021;118(24):1–10. doi:10.1073/pnas.2105465118.
 22. Wei X, Zhang L, Yang Y, Hou Y, Xu Y, Wang Z, Su H, Han F, Han J, Liu P. et al. LL-37 transports immunoreactive cGAMP to activate STING signaling and enhance interferon-mediated host antiviral immunity. *Cell Rep*. May 31 2022;39(9):110880. doi:10.1016/j.celrep.2022.110880.
 23. Cheradame L, Guerrero IC, Gaston J, Schmitt A, Jung V, Goudin N, Pouillard M, Radosevic-Robin N, Modesti M, Judde J-G. et al. STING protects breast cancer cells from intrinsic and genotoxic-induced DNA instability via a non-canonical, cell-autonomous pathway. *Oncogene*. 2021 Dec;40(49):6627–6640. doi:10.1038/s41388-021-02037-4.
 24. Berger G, Knelson EH, Jimenez-Macias JL, Nowicki MO, Han S, Panagioti E, Lizotte PH, Adu-Berchie K, Stafford A, Dimitrakakis N. et al. STING activation promotes robust immune response and NK cell-mediated tumor regression in glioblastoma models. *Proc Natl Acad Sci U S A*. Jul 12 2022;119(28):e2111003119. doi:10.1073/pnas.2111003119.
 25. Gao Y, Zheng X, Chang B, Lin Y, Huang X, Wang W, Ding S, Zhan W, Wang S, Xiao B. et al. Intercellular transfer of activated STING triggered by RAB22A-mediated non-canonical autophagy promotes anti-tumor immunity. *Cell Res*. 2022 Dec;32(12):1086–1104. doi:10.1038/s41422-022-00731-w.